Structure and Properties of Small Molecule−Polymer Blend Semiconductors for Organic Thin Film Transistors

Jihoon Kang,[†] Nayool Shin,[†] Do Young Jang,[†] Vivek M. Prabhu,[*,‡] and Do Y. Yoon[*,†]

Department of Chemistry, Seoul National University, Seoul, 151-747, Korea, and Polymers Division, National Institute of Standards & Technology, Gaithersburg, Maryland 20899

Received June 4, 2008; E-mail: dyyoon@snu.ac.kr; vprabhu@nist.gov

Organic semiconductors are generally regarded to be the most critical element of the new generation of optoelectronic devices such as printable flexible electronics and photovoltaic devices.[1,2] Therefore, organic small molecule and polymer semiconductors[3−5] have been actively investigated to obtain the desired electrical properties. However, their field-effect mobility, solution processability and long-term performance stability must still be substantially improved[6] in order to match conventional amorphous silicon semiconductors whose field-effect mobilities reach as high as ca. 1 cm^2/Vs. Recently, small molecule organic semiconductors have achieved field-effect mobilities over 1 cm^2/Vs due to the intelligent design and synthesis of organic molecules with novel molecular packing structure and high crystallinity.[4,7−9] However, the solution processing of small molecules, necessary for printable electronic devices, encounters serious issues including the nonuniform film thickness and coating problems such as dewetting. In comparison, polymer semiconductors are well suited for the solution-processing because of their excellent film-forming characteristics. But semiconducting polymer films generally show a limited charge carrier mobility (<0.3 cm^2/Vs) and poor performance stability, most likely due to the low crystallinity and the resultant high permeability of moisture and oxidizing species.

A possible solution to this problem was proposed by Brown et al., who applied solution-processed blend films of a semiconducting small molecule and an insulating polymer as the active layer.[10] This approach of combining the advantages of small molecules and polymers led to a stable field-effect mobility over 0.3 cm^2/Vs. It was postulated that the semiconducting small molecules were phase-segregated to the air surface of the thin blend film, since this excellent mobility was reported only for the organic thin film transistor (OTFT) devices with a top-gated structure (Figure 1a). However, no concrete experimental evidence has been presented to support this proposal. Moreover, such a top-gate/bottom-contact OTFT structure presents serious problems for fabricating technologically important devices due to the potential damage to the active layer during the subsequent process steps including the gate electrode patterning and wiring. Instead, a bottom-gate/bottom-contact structure as shown in Figure 1b is strongly favored. For fabricating such structures it is critical to have the segregation of the semiconducting small molecules at the interface with the dielectric substrate in the solution-processed thin blend active layer of ca. 100 nm thickness.

Therefore, the scope of this work is 4-fold. First, we delineated the structural origin of the enhanced performance of the small molecule−polymer blend active layer as reported by Brown et al.[10] Second, we explored a key material parameter, molecular mass of the insulating polymer, which strongly influences the segregation
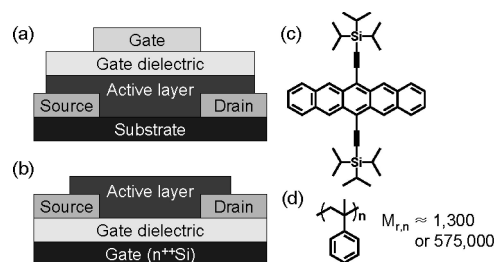
Figure 1. Schematic drawings of (a) top-gate/bottom-contact and (b) bottom-gate/bottom-contact OTFTs, and chemical structures of (c) TIPS-pentacene and (d) poly(α-methylstyrene) (PαMS).

characteristics in thin blend films, so that we could optimize the conditions for the segregation of small molecule semiconductors at the bottom interface with the solid substrate. Third, we investigated the crystalline morphology of small molecule semiconductors in thin blend films in order to determine whether they have the desired molecular packing and orientation. Finally, we characterized the electrical properties of the optimized blend active layer in bottom-gate/bottom-contact OTFT devices, and demonstrated that the optimized blend active layer exhibited superior functional properties (field-effect mobility, on/off ratio, and threshold voltage) over those of neat small molecule system.

For our experiments, we employed blend films of 6,13-bis(triisopropylsilylethynyl)pentacene (TIPS-pentacene) (see Figure 1c) and poly(α-methylstyrene) (PαMS) (see Figure 1d). TIPS-pentacene is a soluble semiconductor known to show a high mobility of 0.17 cm^2/Vs when solution processed upon SiO$_2$ dielectric,[9] and PαMS insulator was shown to work quite well with a variety of small molecule semiconductors.[10]

To obtain the most critical structural information underlying the observed electrical properties of the thin blend active layer, we have carried out neutron reflectivity (NR) experiments which allow the measurements of TIPS-pentacene depth profiles with nanometer-scale resolution. Since this technique relies on the contrast of neutron scattering length density arising primarily from the variation in the hydrogen and deuterium concentration, the NR sensitivity was provided by employing a deuterium-labeled TIPS-pentacene (d-TIPS-pentacene), synthesized as described in the Supporting Information. Therefore, the reflectivity arising from the segregation of d-TIPS-pentacene in the blend film with PαMS could be measured with a sufficiently high precision for accurately determining the d-TIPS-pentacene depth profile.

Measurements were performed on the NG 7 reflectometer at the Center for Neutron Research, National Institute of Standards and Technology (NIST). The specular reflectivity (R) curves, corrected for background, were measured as a function of wave vector (**Q**) normal to the film ($\mathbf{Q} = 4\pi\lambda^{-1} \sin \theta$, where λ is the fixed incident neutron wavelength of 4.75 Å and θ is the angle of reflection) with

† Seoul National University.
‡ National Institute of Standards & Technology.
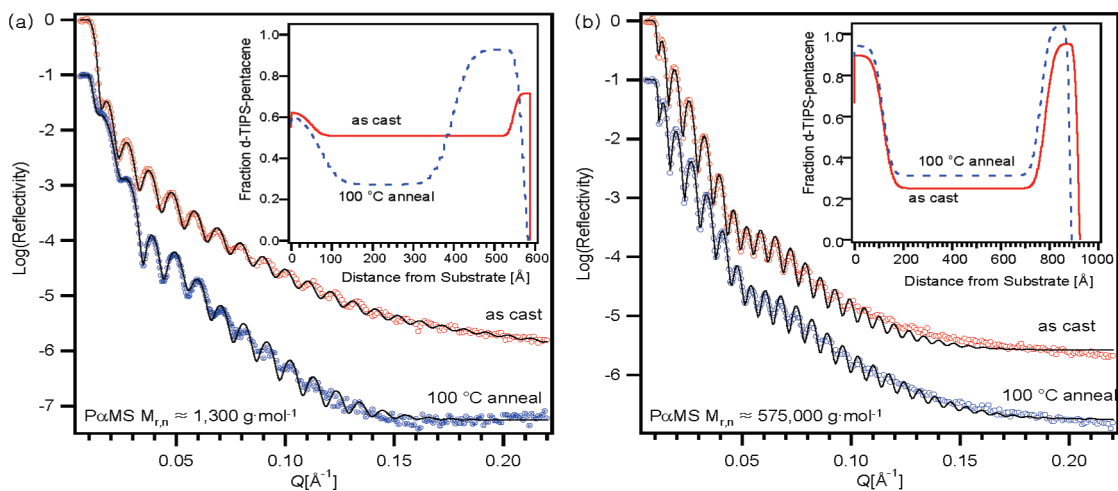
Figure 2. Neutron reflectivity profiles and fitted concentration profiles (in the insets) of d-TIPS-pentacene in the 1:1 ratio (by mass) blend films of d-TIPS-pentacene and PαMS for (a) the blend with PαMS of $M_{r,n} \approx 1300$ g·mol^{-1} and (b) the blend with PαMS of $M_{r,n} \approx 575\,000$ g·mol^{-1} in the as-cast and the annealed (20 min at 100 °C) films. The fitted reflectivity curves from the modeled density profiles are shown by black solid lines.

the resolution $\Delta Q/Q = 0.04$. The reflectivity data were then fit to the results calculated from the modeled depth profiles using the Parratt algorithm, in units of scattering length density (ρ).

Figure 2a shows the specular NR data for the blend films (1:1 ratio by mass) of d-TIPS-pentacene with PαMS of relative number average molecular mass $M_{r,n} \approx 1300$ g·mol^{-1}, spin-cast on thick silicon substrate, for the initial as-cast and vaccuum-dried film and the film subsequently annealed at 100 °C for 20 min in nitrogen atmosphere, respectively. This low molecular-mass PαMS blend system is identical to the system reported by Brown et al.,[10] and thus was chosen to understand the excellent electrical properties they reported. In general, the well-defined oscillating fringes arise from the interference of the reflected neutrons from the air and the substrate interfaces, such that the period of the fringes is inversely proportional to the film thickness. The reflectivity data in Figure 2a indicates that the blend films with the low molecular-mass PαMS exhibit distinctly different features between the as-cast film and the film annealed at 100 °C, as noticed by the appearance of an enveloping longer wavelength profile upon the short wavelength features in the annealed film data. From the fits to the NR data the scattering length density profile $\rho(z)$ was interpreted as d-TIPS-pentacene volume fraction as a function of distance from the substrate using the relation: $\phi_{d\text{-TIPS}} \times \rho_{d\text{-TIPS}} + (1 - \phi_{d\text{-TIPS}}) \times \rho_{P\alpha MS} = \rho_{blend}$, where $\phi_{d\text{-TIPS}}$ corresponds to the volume fraction of d-TIPS-pentacene. Reference pure component films provide the values of $\rho_{d\text{-TIPS}}$ and $\rho_{P\alpha MS}$ as 4.37×10^{-6} Å^{-2} and 1.12×10^{-6} Å^{-2}, respectively. Insets in Figure 2 show the depth profiles of d-TIPS-pentacene for the as-cast film and the film subsequently annealed at 100 °C. In the as-cast film, the blend film with a low molecular-mass PαMS ($M_{r,n} \approx 1300$ g·mol^{-1}) has a mostly uniform distribution of d-TIPS-pentacene with a concentration of 51% by volume throughout the film thickness, except in the two narrow interfacial regions: 11% excess at the blend/silicon substrate and 20% excess at the blend/air interface. Upon annealing this blend film at 100 °C under nitrogen atmosphere, a large-scale restructuring occurred which resulted in a strong segregation of d-TIPS-pentacene at the film/air interface. This segregated film structure consists of nearly pure TIPS-pentacene layer of ca. 177 Å thickness at the air surface, PαMS-rich middle layer of ca. 326 Å thickness, and a slightly TIPS-pentacene enriched layer of ca. 70 Å at the silicon substrate interface. Since the glass transition temperature (T_g) of the PαMS with $M_{r,n} \approx 1300$ g·mol^{-1} is observed around 74 °C, the annealing step at 100 °C allowed sufficient mobility for TIPS-

pentacene to segregate preferentially to the air interface. This segregation feature, as found from the NR experiments, is completely consistent with the excellent field-effect mobility of this blend active layer only in the top-gated OTFT structure, as reported by Brown et al.[10]

As a means of changing the segregation characteristics, we changed the molecular mass of the insulating polymer (PαMS) to a very high value of $M_{r,n} \approx 575\,000$ g·mol^{-1}. Figure 2b shows the corresponding NR data and the depth profiles of d-TIPS-pentacene in the 1:1 ratio (by mass) blend. For this blend with such a high molecular-mass PαMS, a strong interface segregation of TIPS-pentacene occurred at both interfaces in the initial spin-cast film. That is, the phase-segregated structure formed a nearly pure TIPS-pentacene layer not only at the air surface, with ca. 134 Å thickness, but also at the silicon substrate interface with ca. 117 Å thickness. And the annealing step at 100 °C did not cause any substantial change in the segregation profile other than a slight increase in the concentration of TIPS-pentacene at both interfaces, probably due to the high glass transition temperature ($T_g \approx 140$ °C) of this high molecular-mass sample well above the annealing temperature. There appears to be a very slight decrease in the overall PαMS fraction and a small decrease in the total film thickness possibly due to the evaporation of residual solvent.

Most surprising and significant is the observation that in the blend with the high molecular-mass PαMS the segregated nearly pure TIPS-pentacene of ca. 117 Å thickness was obtained at the bottom silicon substrate interface, which was not seen for the blend system with the low molecular-mass PαMS (see Figure 2a). As discussed above, this feature is critically important for fabricating bottom-gate/bottom-contact OTFT structures, provided that the TIPS-pentacene molecules in the segregated thin films form a highly crystalline structure with the $\pi-\pi$ stacked molecular layers oriented parallel to the film surface.[9,11]

Figure 3 shows the grazing-incidence X-ray diffraction (GIXD) patterns, recorded at Pohang Accelerator Laboratory, Korea (PAL) for the thin blend films of TIPS-pentacene and PαMS with $M_{r,n} \approx 575\,000$ g·mol^{-1}, identical to those employed for the neutron reflectivity experiments. Both the as-cast film and the film subsequently annealed at 90 °C show highly crystalline morphology of TIPS-pentacene molecules, with the layer spacing of 16.6 Å, which is in close agreement with 16.8 Å reported by Anthony et al.[12] Moreover, the molecular layers are highly oriented parallel to the film surface (i.e., the normal to the (00*l*) planes oriented along
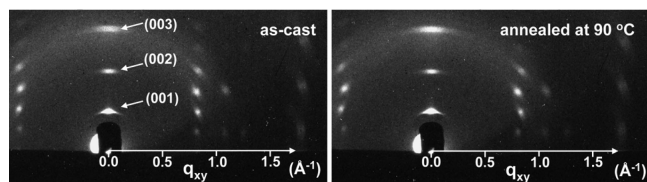
Figure 3. GIXD patterns of spin-cast films of TIPS-pentacene/PαMS ($M_{r,n} \approx 575\,000$ g·mol^{-1}) blend, observed for the as-cast and the 90 °C-annealed films. The scale of the scattering vector is denoted in the film plane by q_{xy}. The (00l) diffraction spots are indicated by the arrows in the figure.
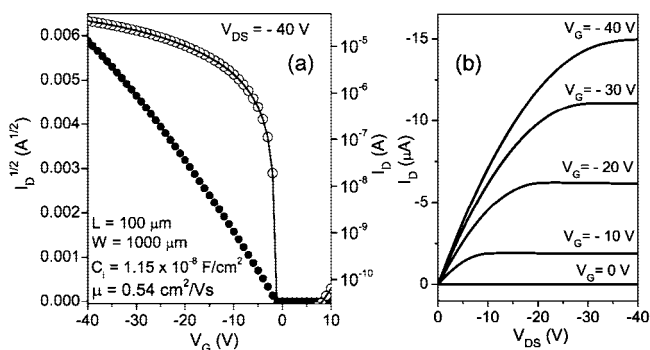
Figure 4. (a) Transfer characteristic and (b) output characteristic of bottom-gate/bottom-contact OTFT with TIPS-pentacene/PαMS ($M_{r,n} \approx 575\,000$ g·mol^{-1}) blend film. The field-effect mobility calculated in the saturation regime is 0.54 cm^2/Vs.

the film thickness (z) direction. As discussed by Anthony and his co-workers,[8,9,11,12] such an orientation is essential to obtaining a high field-effect mobility of TIPS-pentacene active layer in OTFT devices. Therefore, we found that the phase-segregated TIPS-pentacene layers in the blend films with the high molecular-mass PαMS exhibited a highly crystalline structure with the desired crystal orientation on silicon solid substrate.

Figure 4 shows the performance characteristics of an excellent bottom-gate/bottom-contact OTFT device prepared with the TIPS-pentacene blend (1:1 ratio by mass) with the high molecular-mass PαMS of $M_{r,n} \approx 575\,000$ g·mol^{-1}. The OTFT devices were fabricated with thermally grown SiO$_2$ dielectric and the surface-modified (with pentafluorobenzenethiol) Au electrodes. The active layer of neat TIPS-pentacene or the blend with PαMS was deposited by drop-casting, relevant to the ink-jet printing process, from 0.5% (by mass) solution of TIPS-pentacene or the blend solution in toluene, followed by solvent evaporation at 90 °C for 20 min. Neat TIPS-pentacene devices exhibited an average field-effect mobility of 0.05 cm^2/Vs with on/off ratio of 10^5 and threshold voltage $|V_{th}| \approx 4$ V. But they showed a serious problem of large fluctuations of device performance due to the poor film-forming characteristics and variation in crystal-growth behavior in the channel area (length $L = 100$ μm and width $W = 1000$ μm). In comparison, the OTFT devices fabricated with the blend with PαMS of $M_{r,n} \approx 575\,000$ g·mol^{-1} showed a much higher average mobility of 0.3 cm^2/Vs and on/off ratio of 5×10^5, together with a reduced threshold voltage $|V_{th}| < 2$ V (see Figure 4). Moreover, the deposited film quality was nearly uniform and satisfactory in all the fabricated OTFTs, and therefore the device performance variation decreased significantly. As an additional benefit, since the semiconducting layer was encapsulated in situ by the insulating polymer layer (see Figure 2b), an improved stability of the active layer in OTFTs is

expected.[13,14] (See the Supporting Information for more details and comparison with previous works.)

The charge transport in OTFT devices is critically dependent on the thin semiconducting layer less than a few nanometer thickness adjacent to the gate dielectric surface.[15,16] Therefore, the excellent electrical properties of the OTFT devices prepared with the blend active layer arises from the nearly pure TIPS-pentacene layer segregated and crystallized at the bottom substrate interface, as indicated by the results of Figure 2b and Figure 3. Moreover, significant improvements in key performance characteristics (field-effect mobility, on/off ratio, and threshold voltage) of the OTFT devices are most likely due to the important changes in the chemical and physical structure at the semiconductor/dielectric interface, as compared with neat TIPS-pentacene system. This is the topic that is poorly understood at the moment and hence needs much further study, in order to realize successful technological applications of organic semiconductors.

Supporting Information Available: Description of the employed materials and experimental methods (NR, GIXD, OTFT device fabrication). This material is available free of charge via the Internet at http://pubs.acs.org.

References

(1) Dimitrakopoulos, C. D.; Malenfant, P. R. L. *Adv. Mater.* **2002**, *14*, 99–117.
(2) Garnier, F.; Hajlaoui, R.; Yassar, A.; Srivastava, P. *Science* **1994**, *265*, 1684–1686.
(3) McCulloch, I.; Heeney, M.; Bailey, C.; Genevicius, K.; MacDonald, I.; Shkunov, M.; Sparrowe, D.; Tierney, S.; Wagner, R.; Zhang, W.; Chabinyc, M. L.; Kline, R. J.; McGehee, M. D.; Toney, M. F. *Nat. Mater.* **2006**, *5*, 328–333.
(4) Murphy, A. R.; Frechet, J. M. J. *Chem. Rev.* **2007**, *107*, 1066–1096.
(5) Pan, H.; Li, Y.; Wu, Y.; Liu, P.; Ong, B. S.; Zhu, S.; Xu, G. *J. Am. Chem. Soc.* **2007**, *129*, 4112–4113.
(6) Chabinyc, M. L.; Salleo, A. *Chem. Mater.* **2004**, *16*, 4509–4521.
(7) Goldmann, C.; Haas, S.; Krellner, C.; Pernstich, K. P.; Gundlach, D. J.; Batlogg, B. *J. Appl. Phys.* **2004**, *96*, 2080–2086.
(8) Subramanian, S.; Park, S. K.; Parkin, S. K.; Podzorov, V.; Jackson, T. N.; Anthony, J. E. *J. Am. Chem. Soc.* **2008**, *130*, 2706–2707.
(9) Payne, M. M.; Parkin, S. R.; Anthony, J. E.; Kuo, C. C.; Jackson, T. N. *J. Am. Chem. Soc.* **2005**, *127*, 4986–4987.
(10) Brown, B. A.; Veres, J.; Anemian, R. M.; Williams, R. T.; Ogier, S. D.; Leeming, S. W. In *International Application Published Under the Patent Cooperation Treaty*, WO 2005/055248 A2, 2005.
(11) Chen, J.; Subramanian, S.; Parkin, S. R.; Siegler, M.; Gallup, K.; Haughn, C.; Martin, D. C.; Anthony, J. E. *J. Mater. Chem.* **2008**, *18*, 1961–1969.
(12) Anthony, J. E.; Brooks, J. S.; Eaton, D. L.; Parkin, S. R. *J. Am. Chem. Soc.* **2001**, *123*, 9482–9483.
(13) Salleo, A.; Arias, A. C. *Adv. Mater.* **2007**, *19*, 3540–3543.
(14) Goffri, S.; Muller, C.; Stingelin-Stutzmann, N.; Breiby, D. W.; Radano, C. P.; Andreasen, J. W.; Thompson, R.; Janssen, R. A. J.; Nielsen, M. M.; Smith, P.; Sirringhaus, H. *Nat. Mater.* **2006**, *5*, 950–956.
(15) Dinelli, F.; Murgia, M.; Levy, P.; Cavallini, M.; Biscarini, F.; de Leeuw, D. M. *Phys. Rev. Lett.* **2004**, *92*, 116802–4.
(16) Ruiz, R.; Papadimitratos, A.; Mayer, A. C.; Malliaras, G. G. *Adv. Mater.* **2005**, *17*, 1795–1798.

JA804013N